Real-Time Implementation of a Constrained MPC for Efficient Airflow Control in a PEM Fuel Cell

Alicia Arce, Alejandro J. del Real, Carlos Bordons, *Member, IEEE*, and Daniel R. Ramírez

***Abstract*—Fuel cells represent an area of great industrial interest due to the possibility to generate clean energy for stationary and automotive applications. It is clear that the proper performance of these devices is closely related to the kind of control that is used; therefore, a study of improved control alternatives is fully justified. The air-supply control is widely used to guarantee safety and to achieve a high performance. This paper deals with this control loop, proposing and comparing two control objectives aimed at satisfying the oxygen starvation avoidance criterion and the maximum efficiency criterion, respectively. The control architecture is based on a constrained explicit model predictive control (MPC) law suitable for real-time implementation due to its low computational demands. The proposed controller is implemented and evaluated on a 1.2-kW polymer electrolyte membrane or proton exchange membrane fuel-cell test bench, thus obtaining real data which show that the maximum efficiency criterion does not conflict with the starvation avoidance criterion and allows system performance improvements of up to 3.46%. Moreover, experimental results utilizing the explicit MPC approach also show improved transient responses compared to those of the manufacturer's control law.**

***Index Terms*—Air-supply management, explicit model predictive control (MPC), fuel cell, maximum efficiency, oxygen starvation, polymer electrolyte membrane or proton exchange membrane (PEM).**

I. Introduction

FUEL CELLS are considered to be good candidates for clean and efficient electricity generation both in stationary and automotive applications. They are electrochemical devices that generate electrical energy from chemical reactants continuously, while fuel and oxidants are being supplied. The fuel-cell operation requires different auxiliary systems and automatic control strategies that ensure appropriate and safe working conditions. Among the many types of fuel cells, this paper is focused on polymer electrolyte membrane or proton exchange membrane (PEM) fuel cells, which run at low temperature and show fast dynamical response, high power density, small size, low corrosion, and high efficiency and therefore make them suitable for mobile applications [1]–[3]. It is clear that the good performance of these devices is closely related to the kind of control that is used; therefore, a study of improved control alternatives is fully justified.

To ensure proper operation, fuel cells are surrounded by a number of ancillary systems, which are typically the following:

1) cooling circuit, which evacuates the heat produced by the electrochemical reaction that takes place inside the fuel cells;
2) humidification circuit, which has to ensure proper membrane state of hydration;
3) hydrogen and air circuits, in order to maintain an adequate reactant supply.

As for the automatic control area, state-of-the-art research is mainly focused on each of the aforementioned auxiliary circuits. Concerning the cooling circuit, an appropriate coolant flow control design plays an important role in ensuring a highly reliable and efficient operation of the fuel-cell system, particularly for large-scale fuel cells in which there are significant evacuated heat rates. In [4], e.g., the authors propose a classic proportional and integral (PI) controller and a state feedback control for the thermal circuit, reducing the parasitic power dissipated for operation of the air blower and coolant pump.

Regarding the humidification circuit, research in efficient and improved water management strategies is being conducted. In fact, water management is a critical issue for PEM fuel cells, in the sense that an appropriate humidity condition not only improves the performance and efficiency of the fuel cell but can also prevent irreversible degradation of internal composition such as the catalyst or the membrane, thus extending the lifetime of the fuel cells. Accordingly, by using existing mathematical models of different levels of detail, ranging from very complex 3-D models suitable for design purposes [7] to other simpler and control-oriented models [8]–[10], many papers have addressed the water transport phenomena inside the fuel cells [5], [6]. In [11], the authors develop a model predictive control (MPC) law whose objective is to keep cathode water concentration constant. Other works, such as [12], propose a control method to sequentially exhaust each individual cell of a fuel-cell stack system, so that only one cell at any given time has an open exhaust port, thereby ensuring that gas will flow through that cell and therefore guarantee water management required for proper performance.

Among all the ancillary circuits, the air-supply circuit is the most power hungry, typically representing up to 80% of the overall auxiliary consumption and up to 30% of the fuel-cell power during rapid increases in the air flow. In fact, excess oxygen replenishment into the cathode will cause power

Manuscript received March 1, 2009; revised May 22, 2009; accepted July 14, 2009. Date of publication August 18, 2009; date of current version May 12, 2010. This work was supported by the Spanish Ministry of Science and Innovation under Grant DPI2007-66718-c04-01.

The authors are with the Departamento de Ingeniería de Sistemas y Automática, Escuela Superior de Ingenieros, Universidad de Sevilla, 41092 Sevilla, Spain (e-mail: aarce@cartuja.us.es; adelreal@cartuja.us.es; bordons@esi.us.es; danirr@cartuja.us.es).

Color versions of one or more of the figures in this paper are available online at http://ieeexplore.ieee.org.

Digital Object Identifier 10.1109/TIE.2009.2029524

waste, consequently leading to a decrease in the net power of the fuel-cell system. Conversely, if fuel cells are subject to oxygen starvation, the potential of these cells can suffer from an accelerated degradation. In other terms, the air-supply circuit must also maintain correct pressure values inside the cells, as the membranes are designed to work within a certain pressure range. Consequently, in order to perform both energy optimization and energy control in a fuel-cell system, many research projects have been conducted to improve air supply, ranging from simple to very elaborate control laws.

Air-supply control is based on keeping the ratio between the oxygen flow generated by the air pump and the flow consumed due to the electrochemical reaction, denominated oxygen excess ratio or λ_{O_2} [13], at a desired set-point value. This ratio must fulfill the stoichiometric relation required to produce the current demanded; otherwise, a phenomenon called oxygen starvation occurs. This phenomenon implies a fast stack degradation and low power generation. Several studies have addressed this undesired phenomenon, proposing that λ_{O_2} be controlled to prevent oxygen starvation [13], [14].

A first attempt consists of classical feedforward laws [15], but unfortunately lacks robustness. Some other works, such as those reported in [16] and [17], achieve the air-flow rate and pressure control using the linear quadratic Gaussian algorithm, which improves the transient response and shows better disturbance rejection capability compared with other simpler control laws such as PI controllers. Other experimental-result-based approaches which have proved to be promising are those related to adaptive control strategies, such as [18], showing that the adaptive controller is robust to the variation of fuel-cell system dynamics. Fuzzy logic control solutions have also been applied to air-flow control [19], [20]. Other researchers have successfully utilized artificial neural networks [21], [22] to predict the stack voltage and current of commercial PEM fuel-cell systems, showing satisfactory speed and accuracy of the prediction algorithms for the real-time control of the aforementioned application. Furthermore, MPC laws can explicitly account for air-supply circuit constraints, showing very good system performances [23], [24].

In other terms, some authors [25] propose a load governor, which controls the current drawn from the fuel cell at the cost of a slower fuel-cell response to current demand. One way to overcome this problem is to add a rechargeable auxiliary current source such as batteries and ultracapacitors [26]–[29] which can quickly respond to a change in current demand. In cases where an energy storage device is included, the fuel cell does not interact directly with the load; instead, the switching converter and the capacitor decouple the fuel-cell and load currents. In [30], the power system consists of a hybrid fuel-cell/capacitor topology, and the control law is designed to track minimum fuel consumption points for a given load power profile. This is done by controlling the air pump voltage and regulating the fuel-cell current through a dc/dc converter. Some other approaches to the control of the air-supply circuit can be found, such as [31], which proposes a PEM fuel-cell current regulation by fuel feed control, avoiding membrane degradation due to oxygen starvation by a self-draining PEM fuel-cell configuration.

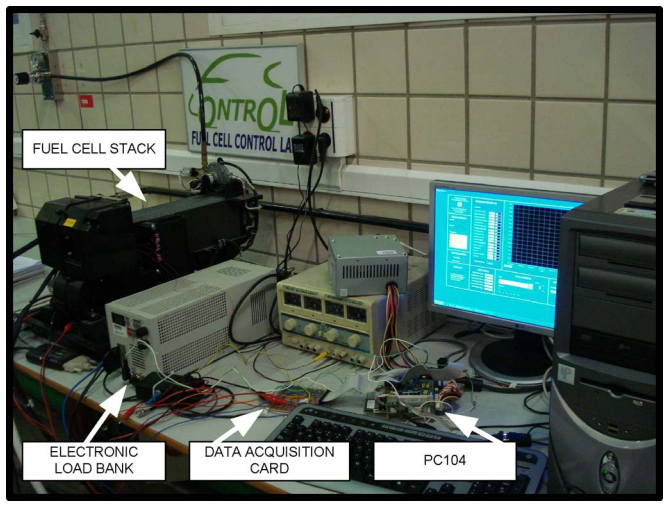

Fig. 1. Fuel-cell test bench.

This paper deals with air-supply system control, underscoring the importance of a subject not properly treated in the literature, which is the real-time implementation of advanced control laws in embedded controllers with relatively low computational performances. In fact, to the best of the authors' knowledge, almost all of the control approaches discussed in the literature are only tested under simulation and implemented in standard computers. In order to test controllers in real circumstances, this paper first develops an MPC approach based on a model fully validated on a 1.2-kW commercial Ballard PEM fuel cell [32]. In a quite novel approach and in order to obtain a controller with low computational demands, an explicit formulation of the MPC control law [33], [34] was obtained, thus allowing its implementation in a real-time platform with its reduced computational capabilities. As another contribution of this paper, such an explicit controller was tested in a test bench with the aforementioned 1.2-kW fuel-cell system, thereby obtaining real data and thus allowing discussion about the attainable performances of real-time control laws for PEM fuel-cell applications. Specifically, faster transient responses and improved efficiencies were observed while comparing the maximum efficiency control objective proposed herein with the manufacturer's control law.

This paper is organized as follows. Section II is dedicated to the experimental setup and test-bench configuration. Control objectives and control architectures are fully explained in Section III. Section IV details the fuel-cell model used by the model-based proposed control laws. The formulation of the constrained explicit controller is shown in Section V. Section VI is dedicated to the experimental result discussions, and finally, some concluding remarks and future work are included in Section VII.

II. Experimental Setup

Experiments were carried on with the test bench shown in Fig. 1. The fuel-cell system is a commercial 1.2-kW Ballard PEM fuel cell, which is currently used by many research groups and is representative of PEM fuel-cell state-of-the-art technology. Fuel-cell power was delivered to a 1-kW resistive

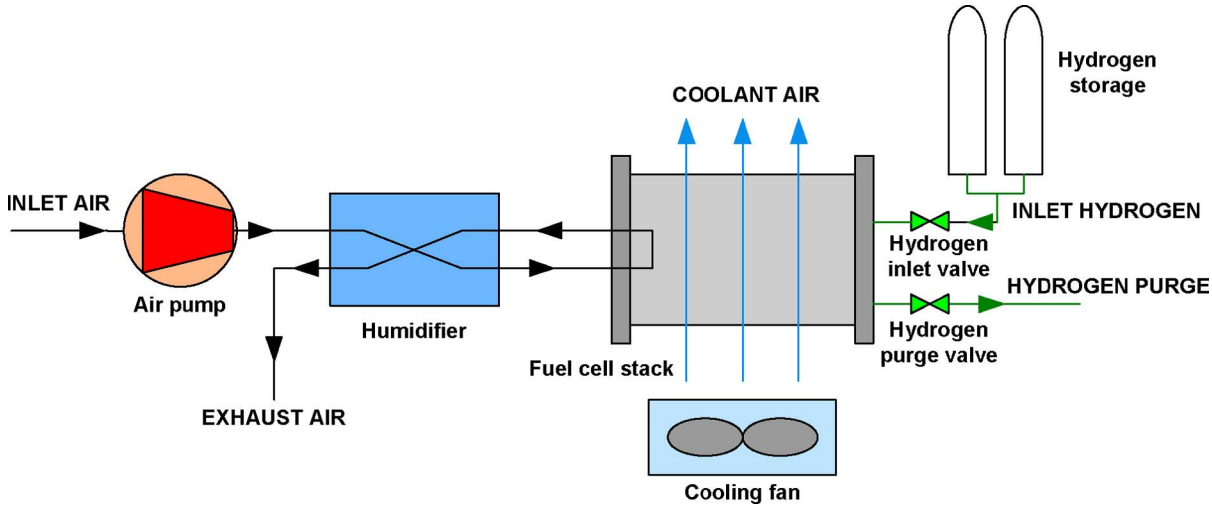

Fig. 2. Fuel-cell system.

electronic load bank. The stack was composed of 46 cells, each with a 110-cm^2 membrane. The fuel-cell system is also composed of an air pump, a humidifier, a cooling fan, and a hydrogen circuit (see Fig. 2). As can be seen, the system is auto-humidified and air cooled by a small fan. The hydrogen feeding of the fuel cell is in *dead-end* mode with flush configuration. Such a benchmark was originally equipped with an onboard controller which assumes air supply, coolant and humidifier circuit control, and safety tasks. In order to implement and test self-made controllers, the original air-supply control was overridden by a PC104 platform with a 650-MHz CPU in which the controllers were programmed.

A. Data Acquisition

The test bench was equipped with a data acquisition card in order to allow communication between the fuel-cell system and the PC104 platform with a configured sampling time of 10 ms, which is sufficient to meet the requirements to the process dynamics (see Section IV). In more specific terms, as shown in Fig. 3, the PC104 receives data from four sensors, corresponding to the stack voltage $V_{\rm st}$, the stack total current $I_{\rm st}$, the net stack current $I_{\rm st,net}$ (which is the result after the subtraction of the parasitic power due to ancillaries from $I_{\rm st}$), and the cathode inlet air flow $W_{\rm cp}$ supplied by the compressor. The $I_{\rm st}$, $V_{\rm st}$, and $W_{\rm cp}$ sensors were already placed in the fuel-cell system by the manufacturer. The $I_{\rm st,net}$ reading was taken by a sensor placed at the electronic load bank used to dissipate the power delivered by the fuel cell. All of these data, as described in the following sections, were used by the control law as feedback in order to calculate the control action, which is the compressor voltage $V_{\rm cp}$.

Once acquired, voltage data from the sensors were correlated with the measurement provided by the manufacturer in order to determine the relationship between the sensor voltages and the corresponding measurements. $I_{\rm st}$, $I_{\rm st,net}$, and $V_{\rm st}$ were identified as linear ratios for the corresponding current sensor. The air flow $W_{\rm cp}$ was identified as a polynomial, which was a function of the corresponding sensor's voltage. Using a least

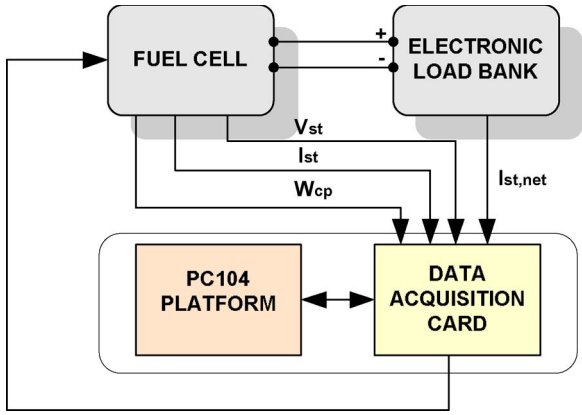

Fig. 3. Data-acquisition configuration.

squares algorithm, the characteristic curve was identified with a third-degree polynomial

$$W_{\rm cp} = 1.862 \cdot V^3_{\rm cp,sensor} + 1.48 \cdot V^2_{\rm cp,sensor} + 2.65 \cdot V_{\rm cp,sensor} \quad (1)$$

where $V_{\rm cp,sensor}$ is the measurement of the voltage sensor placed at the air inlet stream flow. Fig. 4 shows a comparison of the identified characteristic curves and the measurements provided by the manufacturers.

B. Data Filtering

Due to the high level of the noise component, some data were filtered. Concretely, $I_{\rm st}$ and $W_{\rm cp}$ were softened by the next digital low-pass filter. The results are shown in Fig. 5

$$G(z) = \frac{0.2835}{z - 0.7165}. \quad (2)$$

C. Data Estimation

The air-supply management of a PEM fuel cell is usually focused on the control of the oxygen excess ratio $\lambda_{\rm O_2}$ inside the cells. Generally, the oxygen excess ratio can be defined as the ratio between the oxygen entering the cathode $(W_{\rm O_2,ca,in})$ and the oxygen reacting in the fuel-cell stack $W_{\rm O_2,reacted}$. Thus,

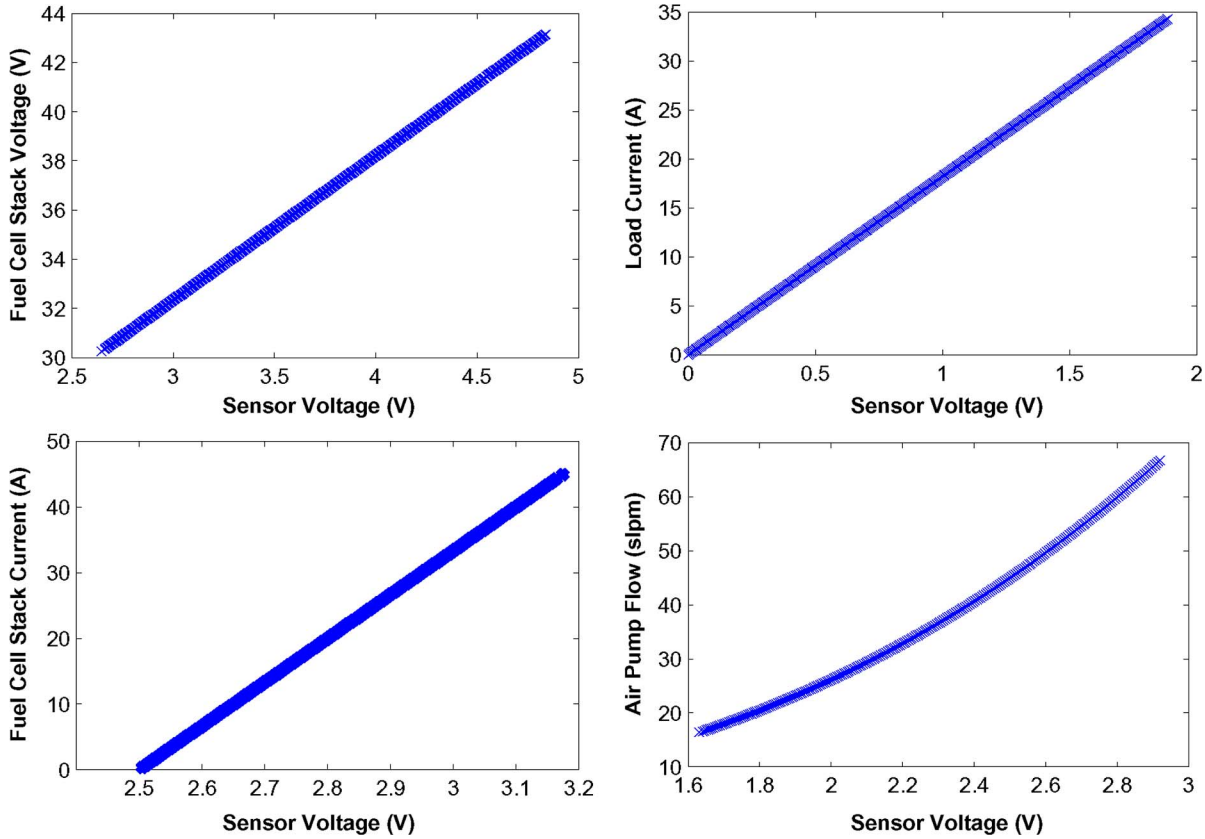

Fig. 4. Sensor data correlations.

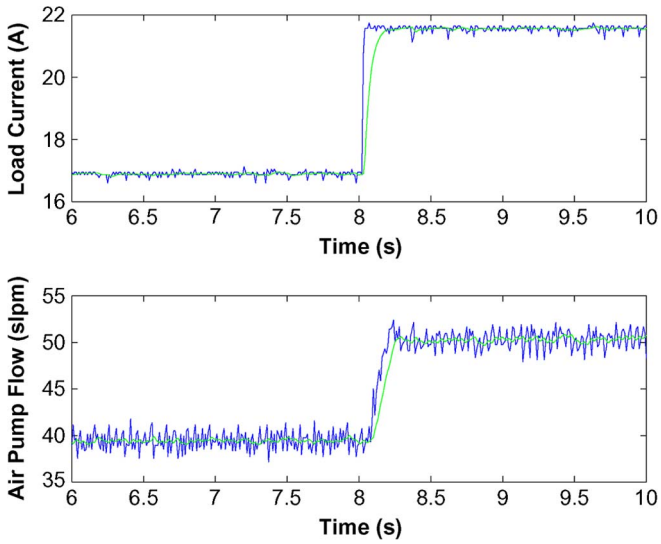

Fig. 5. Data filtering.

λ_{O_2} is considered as a performance variable of the system, and its regulation is an important issue since this parameter is related to the safety of the fuel cell. The oxygen excess ratio is defined as [15]

$$\lambda_{O_2} = \frac{W_{O_2,ca,in}}{W_{O_2,reacted}}. \tag{3}$$

As λ_{O_2} is difficult to measure, its value must be estimated using the available data W_{cp} and I_{st} taken by sensors. Thus, the oxygen mass flow rate can be defined as a function of the mass flow rate of dry air $W_{a,ca,in}$ at the cathode inlet

$$W_{O_2,ca,in} = x_{O_2,ca,in} \cdot W_{a,ca,in}. \tag{4}$$

The oxygen mass fraction $x_{O_2,ca,in}$ can be calculated by

$$x_{O_2,ca,in} = \frac{y_{O_2,ca,in} \cdot M_{O_2}}{y_{O_2,ca,in} \cdot M_{O_2} + (1 - y_{O_2,ca,in}) \cdot M_{N_2}} \tag{5}$$

where M_{O_2} and M_{N_2} denote the molar masses of oxygen and nitrogen, respectively. For the oxygen mole fraction, a value of $y_{O_2,ca,in} = 0.21$ is assumed. The mass flow rate of dry air at the cathode inlet is defined as

$$W_{a,ca,in} = \frac{1}{1 + \omega_{ca,in}} \cdot W_{cp} \tag{6}$$

with the humidity ratio

$$\omega_{ca,in} = \frac{M_v}{M_{a,ca,in}} \cdot \frac{p_{v,ca,in}}{p_{a,ca,in}} \tag{7}$$

and the air molar mass at the cathode inlet

$$M_{a,ca,in} = y_{O_2,ca,in} \cdot M_{O_2} + (1 - y_{O_2,ca,in}) \cdot M_{N_2}. \tag{8}$$

The vapor pressure $p_{v,ca,in}$ and the dry air pressure $p_{a,ca,in}$ used to calculate the humidity ratio $\omega_{ca,in}$ are defined as

$$p_{v,ca,in} = \phi_{ca,in} p_{sat}(T_{ca,in}) \tag{9}$$

$$p_{a,ca,in} = p_{ca,in} - p_{v,ca,in} \tag{10}$$

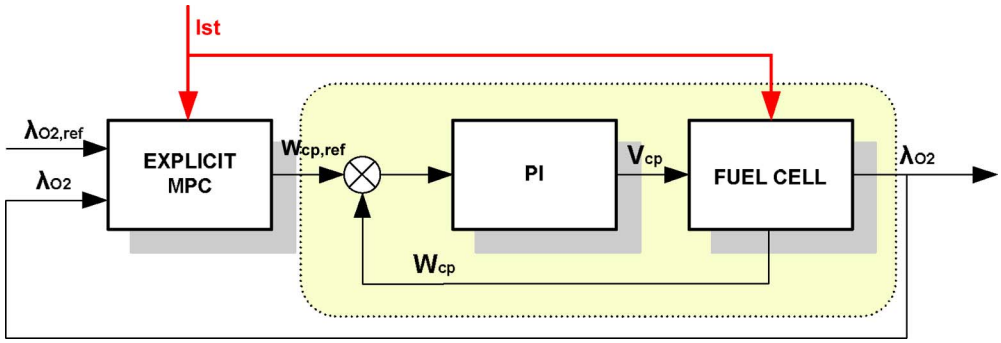

Fig. 6. Control architecture for a fixed λ_{O_2}.

with $\phi_{\mathrm{ca,in}}$ denoting the relative humidity of air at the cathode inlet. $p_{\mathrm{sat}}(T_{\mathrm{ca,in}})$ and $p_{\mathrm{ca,in}}$ represent the vapor saturation pressure at a certain temperature and the pressure at the cathode inlet, respectively.

The rate of oxygen consumption is proportional to the current withdrawn from the fuel cell and can be written as [35]

$$W_{\mathrm{O_2,reacted}} = M_{\mathrm{O_2}} \cdot \frac{n \cdot I_{\mathrm{st}}}{4 \cdot F} \tag{11}$$

with $n = 46$ as the number of cells of the fuel-cell stack utilized and F as the Faraday constant.

In order to refer only to variables which can be measured, some simplifications can be made: The temperature at the cathode inlet $T_{\mathrm{ca,in}}$ is assumed to be equal to the ambient temperature, and the relative humidity is assumed to be equal to 1. In order to consider the simplification regarding the temperature at the cathode inlet, a study aimed at evaluating the associated errors was conducted. Thus, the temperature increment due to the pressure increment downstream from the compressor can theoretically be calculated as

$$T_{\mathrm{cp,out}} = T_{\mathrm{cp,in}} + \frac{T_{\mathrm{cp,in}}}{\eta_{\mathrm{cp}}} \left[\left(\frac{p_{\mathrm{cp,out}}}{p_{\mathrm{cp,in}}} \right)^{\frac{\gamma-1}{\gamma}} - 1 \right] \tag{12}$$

where $T_{\mathrm{cp,out}} = T_{\mathrm{ca,in}}$ is the temperature of the air leaving the compressor (i.e., the air entering the cathode), $T_{\mathrm{cp,in}} = T_{\mathrm{amb}}$ is the temperature of the air entering the compressor, $\eta_{\mathrm{cp}} = 0.85$ is the compressor efficiency, $p_{\mathrm{cp,out}} = p_{\mathrm{ca,in}}$ is the compression ratio with $p_{\mathrm{cp,out}} = p_{\mathrm{ca,in}}$ being the cathode inlet air pressure, $p_{\mathrm{ca,in}} = 1$ bar, and $\gamma = 1.4$, which is the specific heat ratio of the air at a constant pressure. The maximum pressure increment ratio given by the Nexa 1.2-kW PEM fuel-cell compressor is approximately 1.1, which causes a maximum theoretical temperature increment of approximately 10 K for an ambient temperature range of 273 K to 320 K. Moreover, a temperature increment of 8.1 K was experimentally measured for an ambient temperature of 299.7 K, utilizing a temperature sensor provisionally placed downstream from the compressor.

Such a maximum temperature increment has a negligible effect on λ_{O_2} estimation, with maximum errors being approximately 0.5%. This simplification can be done due to the little pressure increment downstream from the compressor. Larger PEM fuel cells require bigger compressors, with larger pressure increments. In such cases, the temperature simplification done herein would result in higher estimation errors; thus, the temperature increment needs to be taken into account.

The pressure at the cathode inlet can also be approximated by identifying the stationary pressure $p_{\mathrm{ca,in}}$ dependence of both measured values W_{cp} and I_{st}

$$p_{\mathrm{ca,in}} \simeq 1.033 + 2.1 \times 10^{-3} \cdot W_{\mathrm{cp}} - 475.7 \times 10^{-6} \cdot I_{\mathrm{st}}. \tag{13}$$

Although the cathode inlet pressure also depends on the air pressure inside the cathode, the aforementioned approximation was made because this pressure was unmeasured. As previously discussed and published in [36], the cathode inlet pressure dynamics depend mainly on the applied airflow W_{cp} dynamics, which means that the associated errors of this approximation are negligible.

III. Control Objectives

As seen in Section II-C, the excess oxygen ratio provides a great deal of information about the fuel-cell safety and performance. In order to avoid oxygen starvation, λ_{O_2} should be kept higher than one and, preferentially, at values higher than two [13]. In fact, oxygen partial pressure falling below such a critical level at any location on the cathode results in a rapid cell voltage decrease and can cause a burn through the surface of the membrane. Furthermore, during abrupt load changes, the air-flow equipment requires time to provide the new amount of air required to maintain λ_{O_2} safety levels, as the electrochemical dynamics of a fuel cell are several orders of magnitude higher than fluid-dynamics response time. Hence, the primary objective of an air-flow controller should be the avoidance of oxygen starvation, assuring safe λ_{O_2} levels and rapid transient response required to recover from abrupt load changes. In this paper, such an objective is accomplished by the control architecture shown in Fig. 6.

The main objective of the aforementioned architecture is to maintain a fixed λ_{O_2} value that ensures the best possible transient response. As shown in Fig. 6, the controller is designed in a master–slave configuration in order to improve the air-flow disturbance rejection capability of the architecture, the master controller being an explicit MPC (whose formulation is detailed in Section V) and the slave being a PI controller. In the proposed configuration, the master controller receives the reference $\lambda_{O_2,\mathrm{ref}}$, the estimation λ_{O_2}, and the stack current

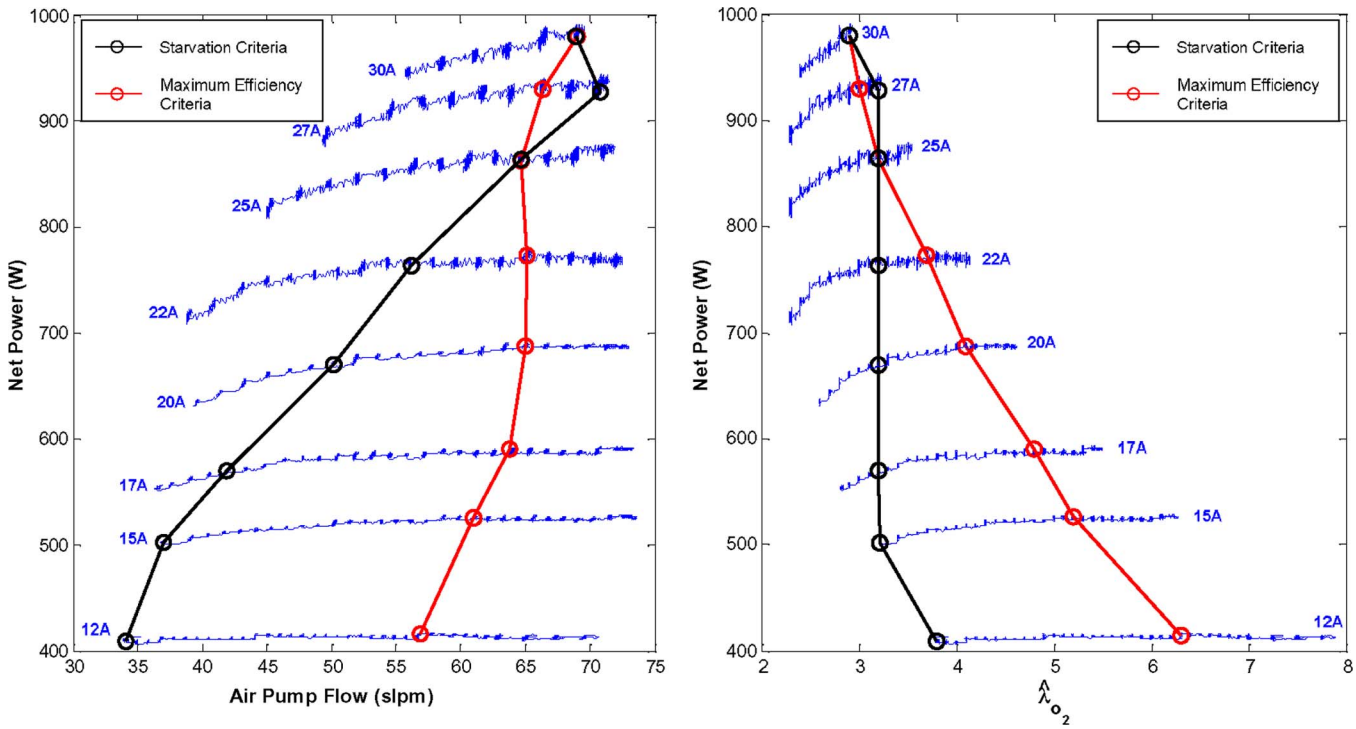

Fig. 7. Steady-state curves and trajectories of the control objectives.

measurement $I_{\rm st}$ (treated as a measurable disturbance) in order to calculate the optimal air-flow rate $W_{\rm cp,ref}$. The slave PI receives such an air-flow reference and calculates the control action $V_{\rm cp}$ also taking the air-flow measured feedback $W_{\rm cp}$ into account.

While fulfilling the first objective, a secondary objective to improve the system efficiency can also be attained. Such an objective was proposed in [37] and is based on the maximization of fuel-cell net power, which is defined as the difference between the power generated by the fuel-cell stack $P_{\rm st} = V_{\rm st}\ I_{\rm st}$ and the power $P_{\rm aux}$ used by the compressor, air fan, and other auxiliary equipment. Hence, the net power can be written as

$$P_{\rm net} = P_{\rm st} - P_{\rm aux} = V_{\rm st} \cdot I_{\rm st,net}. \tag{14}$$

The left graph in Fig. 7 shows an experimental relation obtained from the Ballard 1.2-kW fuel cell between the net power $P_{\rm st,net}$ and the air flow $W_{\rm cp}$ for different stack currents $I_{\rm st}$. Starting from a low air-flow rate, it can be observed that the net power increases with an increasing air-flow rate. After reaching the maximum net power for a certain stack current, a further increase of the air-flow rate leads to a reduction in the net power. In fact, higher λ_{O_2} values imply that the compressor consumes more power, which penalizes the fuel-cell power. However, such high λ_{O_2} values also imply that the fuel cell is working in a more efficient region; therefore, power losses decrease. The overall power balance results in a higher fuel-cell net power for a fixed fuel-cell current, which results in a more efficient system.

A similar graph can be obtained by estimating λ_{O_2} as described in Section II-C, thus showing the relation between the net power and the oxygen excess ratio for various stack currents (right graph in Fig. 7). As shown, there is an optimal λ_{O_2} value for each current density value. The first and second objective steady-state paths are shown in Fig. 7. Due to the limited compressor's operative range, there are correspondingly limited ranges in low and high currents where the fixed $\lambda_{O_2} = 3.2$ could not be reached. Notice that the secondary objective does not conflict with the primary objective, as the optimal λ_{O_2} values are higher than the "safe" λ_{O_2} values for every stack current. Such a result makes it possible to improve the control architecture shown in Fig. 6 by including a reference governor which acts as a feedforward controller and calculates an optimal λ_{O_2} reference value for the explicit MPC master controller, which is determined by the stack current (see Fig. 8).

This paper can be generalized for all PEM fuel cells. In fact, this paper is based on [38] in which such strategies were successfully elaborated for a 75-kW PEM fuel cell. The reason is that all the curves presented in [38] have similar shapes for all PEM fuel cells, resulting in the aforementioned generalization.

IV. Control-Oriented Model

There are many PEM fuel-cell models in the literature. In fact, many models have been developed in the last 15 years. Earlier models, such as [39], presented an empirical polarization curve based on calculated coefficients, as some recent papers [40] have shown. In [15], an extended equation, with a larger number of parameters was proposed, improving the formulation of polarization curve dependence on the stack temperature and on hydrogen and oxygen partial pressures. As the polarization curve had initially been based solely on the steady-state case, recent research has considered the fluid dynamics inside the stack, taking transient behavior into account. Some authors have proposed complex multidimensional studies [41], [42]. Although these contributions are very useful for

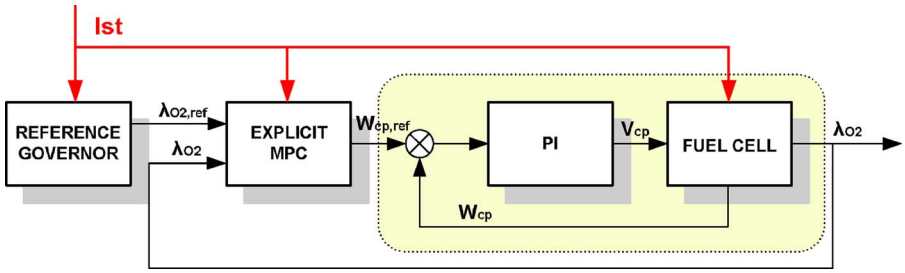

Fig. 8. Control architecture for maximum efficiency.

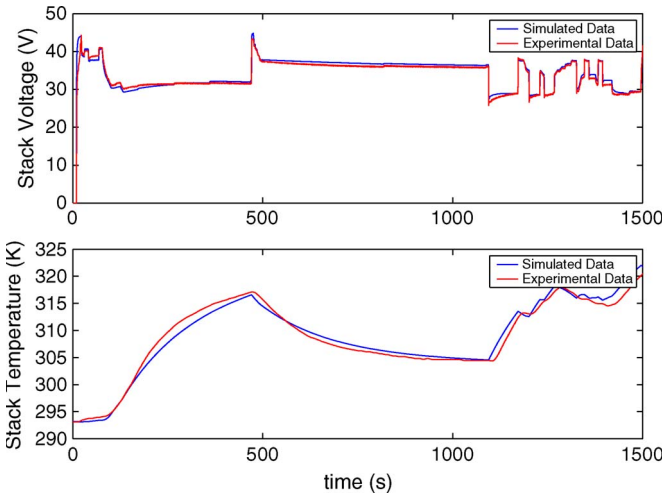

Fig. 9. Experimental validation of the fuel-cell model.

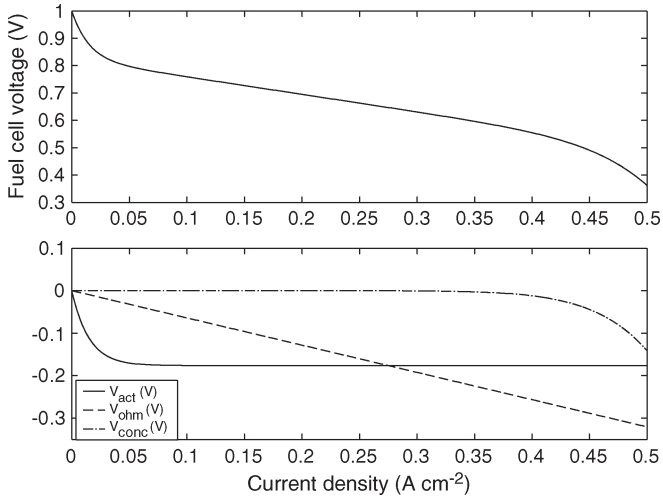

Fig. 10. Fuel-cell polarization curve and voltage drop contributions.

fuel-cell design, they require large computational calculations. Thus, simplified 1-D models are more suitable for control purposes, such as those presented in [15] and [43] and the nonlinear model developed by the authors of this paper [32]. As validated models in the literature are scarce, mainly due to the complexity and cost of fuel-cell test benches, one of the main novelties of the aforementioned model consists of its validation with real results observed in the 1.2-kW Ballard PEM fuel cell which is the object of this paper, which demonstrates the accuracy of the proposed model methodology (as shown in Fig. 9).

In such a control-oriented model, theoretical equations are combined with experimental relations, resulting in a semiempirical formulation. It is composed of three main modules: electrochemical static model, fluid-dynamics model, and thermal dynamics model. With respect to the electrochemical static model, the voltage supplied by a fuel cell is evaluated by curves that present the voltage of the cells $V_{\rm fc}$ versus the current density

$$V_{\rm fc} = v_0 - v_{\rm act} - v_{\rm ohm} - v_{\rm conc} \tag{15}$$

where v_0 is the open circuit voltage, which falls as the current supplied by the stack increases. Thus, in the first stage, up to a certain current value, activation overvoltage drops $(v_{\rm act})$ prevail, as a result of the need to move electrons and to break and form chemical bonds. At a latter stage, as current density rises, ohmic losses $(v_{\rm ohm})$ prevail. They are derived from membrane resistance to transfer protons and form the electrical

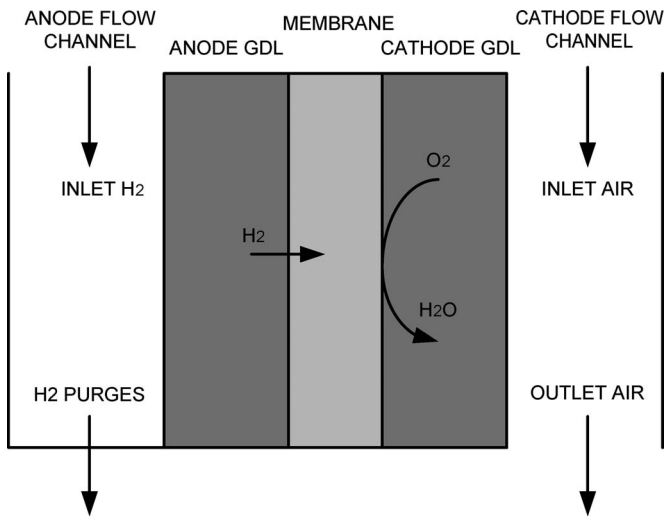

Fig. 11. Fluid-dynamics model subblocks.

resistance of the electrodes to transfer electrons. When the current is very high, at a maximum power level, concentration overvoltage $(v_{\rm conc})$ produces a quick drop of the voltage due to internal inefficiencies at high levels of reactive consumption. In Fig. 10, the polarization curve that corresponds to a single cell of the 1.2-kW stack modeled here can be seen. The drops described previously are case adapted as well.

As for the fluid-dynamics block, it is composed of five interconnected subblocks, which correspond to the control volumes of the two flow channels, the diffusion gas layers of the cathode

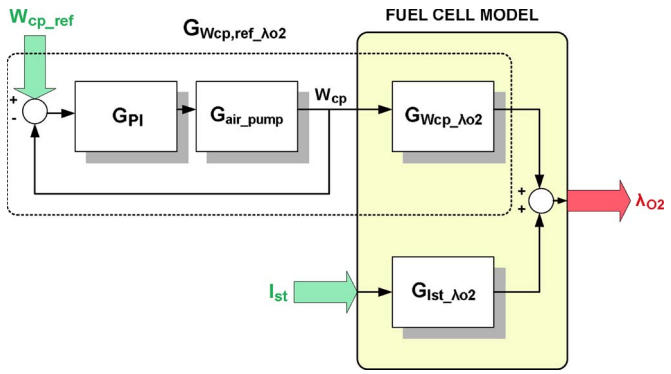

Fig. 12. Input–output of the linearized model.

and anode, and the transport of chemical species across the membrane (see Fig. 11).

Finally, an energy balance is done in order to obtain the thermal model, taking into account the energy produced by the chemical reaction of water formation (which is supposed to be formed as water steam) $H_{\rm reac}$, the energy supplied in the form of electricity $P_{\rm elec}$, and the amount of heat evacuated by radiation $Q_{\rm rad,B2amb}$ and both natural and forced convection $Q_{\rm conv,B2amb}$. As for the 1.2-kW Ballard PEM fuel cell discussed herein, heat removal is completed through forced convection by a small fan. In bigger fuel-cell stack systems, where the amount of heat is considerably larger, water cooling in necessary. In those cases, the forced convection term should take into account the heat exchange in cooling fluid

$$m_{\rm st}C_{\rm st}\frac{{\rm d}T_{\rm st}}{{\rm d}t} = \dot{H}_{\rm reac} - P_{\rm elect} - \dot{Q}_{\rm rad,B2amb} - \dot{Q}_{\rm conv,B2amb} \tag{16}$$

where $m_{\rm st}$ is the fuel-cell stack mass, $C_{\rm st}$ is the average heat capacity of the system, and $T_{\rm st}$ is the average fuel-cell temperature. A more detailed description of such a model including all the equations and parameters can be found in [32], as the scope of this paper includes the control architecture description but not the modeling issues.

As will be discussed in Section V, the explicit predictive control law proposed herein is based on a controller autoregressive integrated moving average (CARIMA) prediction model and thus requires a linearized fuel-cell model. In more specific terms, the process "seen" by the explicit MPC can be modeled by a single-input–single-output model with a measured disturbance (see Fig. 12), in which the input is the inlet air flow $W_{\rm cp}$, the output is the oxygen excess ratio $\lambda_{\rm O_2}$, and the stack current $I_{\rm st}$ is the disturbance. Such a model can be obtained by linearizing the aforementioned nonlinear model presented in [32] around an operation point, while also taking into account the fact that the PI which controls the compressor was set up with a proportional constant $K = 0.7$ and an integral constant

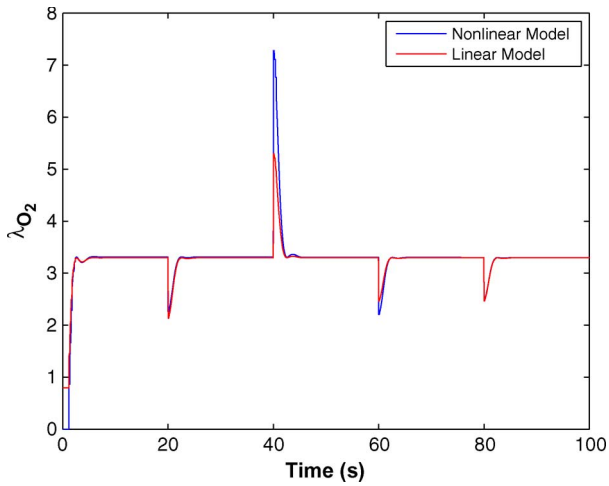

Fig. 13. Comparison between linear and nonlinear models.

$T_I = 100$, resulting in the following PI controller transfer function $G_{\rm PI}(s)$:

$$G_{\rm PI}(s) = \frac{70 \cdot s + 0.7}{100 \cdot s}. \tag{17}$$

Specifically, the operating current was set at 20 A, which is the mean value of the whole range. Setting an oxygen excess ratio of 3.5, which is a value included in normal operating ranges, results in an air inlet flow operating point of 53.5 slpm. Taking all these assumptions into account, the process model on which the explicit MPC is based can be described by the transfer functions (18) and (19), as shown at the bottom of the page.

Applying the rule of thumb for choosing a sampling time ten times lower than the fastest dynamic of the process and so as to obtain a discrete time model, a sampling time of 10 ms was chosen, resulting in the transfer functions (20) and (21), as shown at the bottom of the next page.

Fig. 13 shows the comparison between the nonlinear model and the discrete linear model. Note that the linear model performs qualitatively close to the nonlinear model, showing discrepancies that can be assumed for control purposes.

V. Formulation of the Explicit Predictive Controller

In this section, the formulation for the explicit predictive controller is presented. It is based on the generalized predictive control (GPC) formulation [44]. The objective of any predictive controller is to compute the future control sequence $u_k, u_{k+1}, \ldots, u_{k+N-1}$ in such a way that the optimal j-step predictions $y_{k+j|k}$ are driven close to the set-point sequence $w_k, w_{k+1}, \ldots, w_{k+N-1}$ for the prediction horizon. As

$$G_{V_{\rm cp,ref},\lambda_{\rm O_2}}(s) = \frac{-7.306 \cdot s^4 \cdot +230.4 \cdot s^3 + 9.848 \times 10^5 \cdot s^2 + 1.848 \times 10^8 \cdot s + 1.944 \times 10^9}{s^5 + 178.4 \cdot s^4 + 4.153 \times 10^4 \cdot s^3 + 2.727 \times 10^6 \cdot s^2 + 1.082 \times 10^8 \cdot s + 9.569 \times 10^8} \tag{18}$$

$$G_{I_{\rm st},\lambda_{\rm O_2}}(s) = -0.1759 \tag{19}$$

model-based control laws are usually computationally demanding, real-time implementation in relatively low performance hardware architectures is not possible. To overcome this problem, explicit formulations like the one described herein are aimed at switching from online to offline computations; therefore, the computed control algorithm execution time turns out to be shorter than the sampling time of the system.

The j-step predictions are computed using a CARIMA prediction model with an extra input for a measured disturbance v

$$A(z^{-1})\cdot y_k = B(z^{-1})\cdot u_{k-1} + D(z^{-1})\cdot v_k + \frac{1}{\Delta}\cdot C(z^{-1})\cdot e_k \tag{22}$$

where $\Delta = 1 - z^{-1}$. The polynomials for the oxygen excess ratio control case are obtained from the discrete transfer functions obtained from (20) and (21). The system output is the oxygen excess ratio (λ_{O_2}), the system input is the air-flow rate in standard liters per minute (W_{cp}), and the measurable disturbance corresponds to the stack demand current (I_{st}).

The way the system approaches the desired trajectories will be indicated by a function J which depends on present and future control signals and disturbances

$$J = \sum_{j=N_1}^{N_2} (y_{k+j|k} - w_{k+j})^2 + \lambda \cdot \sum_{j=1}^{N_u} (\Delta u_{k+j-1})^2 \tag{23}$$

where N_1 and N_2 define the beginning and end of the cost horizon, N_u is the control horizon, and $y_{k+j|k}$ is the output prediction for time $k+j$ made at time k. The control signal is assumed to be constant after the control horizon, and the future measured disturbances are supposed to be constant and equal to the last measured value.

The j-step predictions can be grouped in a vector $\mathbf{y} = [y_{k+N_1|k} \cdots y_{k+N_2|k}]^{\mathrm{T}}$ that can be computed from the following prediction equation (see [44]):

$$\mathbf{y} = G\cdot\mathbf{u} + F_x\cdot x \tag{24}$$

where $G \in \Re^{N\times N_u}$, $\mathbf{u} = [\,\Delta u_k \quad \cdots \quad \Delta u_{k+N_u-1}\,]^{\mathrm{T}}$, $F_x \in \Re^{N\times \mathbf{d}\mathrm{imx}}$, $N = N_2 - N_1$, and $x \in \Re^{\mathbf{d}\mathrm{imx}}$. The first term $G\cdot\mathbf{u}$ represents the forced response and the second $F_x\cdot x$ the free response (see [44]). The parameter vector x contains the present and past values of y_k and the past values of Δu_k and Δv_k on which the free response of the system depends. In the context of a CARIMA model, vector x represents the process state. For the fuel-cell control model, this vector is represented by

$$x = [y_k \ \cdots \ y_{k-4} \ \ \Delta u_{k-1} \ \cdots \ \Delta u_{k-3} \ \ \Delta v_{k-1} \ \cdots \ \Delta v_{k-4}]^{\mathrm{T}}. \tag{25}$$

With prediction equation (24), the cost function can be rewritten as

$$J(\mathbf{u},\mathbf{w},x) = (G\cdot\mathbf{u} + F_x\cdot x - \mathbf{w})^{\mathrm{T}}\cdot(G\cdot\mathbf{u} + F_x\cdot x - \mathbf{w}) + \lambda\cdot\mathbf{u}^{\mathrm{T}}\cdot\mathbf{u} \tag{26}$$

where $\mathbf{w} = [\,w_{k+N_1} \quad \cdots \quad w_{k+N_2}\,]^{\mathrm{T}}$. The optimal control sequence will be computed by solving, at each sampling time, the following quadratic programming (QP) problem:

$$\mathbf{u}^* = \arg\min_{\mathbf{u}\in U} J(\mathbf{u},\mathbf{w},x) \tag{27}$$

where $U \triangleq \{\forall\mathbf{u} : R\cdot\mathbf{u} \le b + S_x\cdot x\}$ with $R \in \Re^{q\times N_u}$, $b \in \Re^{q\times 1}$, and $S_x \in \Re^{q\times \mathbf{d}\mathrm{imx}}$ is the convex set of all the feasible control sequences. Note that the constraints on the output, control moves, and control-signal-amplitude values can be easily written in this form [44]. Moreover, the constraints on the amplitude of the control signal imply that the definition of U must be updated at each sampling time (specifically, u_{k-1} must be included in the computation of b; see [44]).

Problem (27) can be rewritten as an equivalent multiparametric QP (mpQP) problem [33], [34]

$$\min \quad \frac{1}{2}\cdot\mathbf{u}^{\mathrm{T}}\cdot Q\cdot\mathbf{u} + \theta^{\mathrm{T}}\cdot C^{\mathrm{T}}\cdot\mathbf{u} \tag{28}$$

$$\text{s.t.} \quad R\cdot\mathbf{u} \le b + S_\theta\cdot\theta \tag{29}$$

where θ is an augmented vector of parameters

$$\theta = [\,x \quad w_{k+N_1} \quad \cdots \quad w_{k+N_2} \quad u_{k-1}\,]^{\mathrm{T}}. \tag{30}$$

The last parameter u_{k-1} is included in θ to allow constraints on the amplitude of the control signal. Note that the dimension of θ can be kept as low as possible if the set-point value is assumed to be constant over the prediction horizon. This assumption is employed in this paper and thus

$$\theta \in \Re^{(\mathbf{d}\mathrm{imx}+2)\times 1} = [\,x \quad w_{k+N_1} \quad u_{k-1}\,]^{\mathrm{T}}. \tag{31}$$

Under this assumption, the matrices in (28) and (29) can be computed as

$$Q = 2\cdot(G^{\mathrm{T}}\cdot G + \lambda\cdot I_{N\times N_u}) \tag{32}$$

$$C = 2\cdot G^{\mathrm{T}}\cdot[\,F_x \quad [-1 \quad \cdots \quad -1]^{\mathrm{T}}_{1\times N} \quad [0 \quad \cdots \quad 0]^{\mathrm{T}}_{1\times N}\,]. \tag{33}$$

$$G_{V_{\mathrm{cp,ref}},\lambda_{\mathrm{O}_2}}(z) = \frac{0.1336\cdot z^4 + 0.3538\cdot z^3 - 0.4232\cdot z^2}{z^5 - 2.101\cdot z^4 + 1.811\cdot z^3 - 1.077\cdot z^2 + 0.5665\cdot z - 0.1679} \tag{20}$$

$$G_{I_{\mathrm{st}},\lambda_{\mathrm{O}_2}}(z) = -0.1759 \tag{21}$$

The system studied has some physical constraints that must be taken into account during the optimization. The input and output amplitudes are limited by minimum and maximum values, and these constraints can be written as

$$T \cdot \mathbf{u} \leq U_{\max} \cdot \mathbf{1}^{N_u \times 1} + [\mathbf{0}^{N_u \times \mathbf{dimx}} \quad -\mathbf{1}^{N_u \times 1}] \cdot \theta \quad (34)$$

$$-T \cdot \mathbf{u} \leq -U_{\min} \cdot \mathbf{1}^{N_u \times 1} + [\mathbf{0}^{N_u \times \mathbf{dimx}} \quad \mathbf{1}^{N_u \times 1}] \cdot \theta \quad (35)$$

$$G \cdot \mathbf{u} \leq y_{\max} \cdot \mathbf{1}^{N \times 1} + [-F_x \quad \mathbf{0}^{N \times 2}] \cdot \theta \quad (36)$$

$$-G \cdot \mathbf{u} \leq -y_{\min} \cdot \mathbf{1}^{N \times 1} + [F_x \quad \mathbf{0}^{N \times 2}] \cdot \theta \quad (37)$$

where $T \in \Re^{N_u \times N_u}$ is a lower triangular matrix of ones and $\mathbf{0}$ and $\mathbf{1}$ are zero matrices and one vectors, respectively. Equations (34) and (35) show the constraints regarding the input physical limitations. Equations (36) and (37) refer to output range limits. All the constraints can be grouped in the form of (29).

The control law defined by the optimization problem presented in (28) and (29) is continuous and piecewise affine [33], [34]. The solution of the mpQP problem yields an explicit description of the control law in the box $\theta_{\min} \leq \theta \leq \theta_{\max}$, in such a way that the optimal value of Δu_k can be obtained by

$$\Delta u_k = f(\theta) \quad (38)$$

$$f(\theta) = F^i \cdot \theta + g^i, \qquad \text{if } H^i \cdot \theta \leq k^i;\ i = 1, \ldots, N_{\text{mpc}} \quad (39)$$

where the polyhedral sets $\{H^i \cdot \theta \leq k^i\}$, $i = 1, \ldots, N_{\text{mpc}}$, are a partition of the given set of parameters θ, F^i, and g^i, which are optimizer gains, and N_{mpc} is the number of regions. The simplest way to implement the piecewise affine feedback law (39) is to store the polyhedral cells $\{H^i \cdot \theta \leq k^i\}$ and perform an online linear search through them to locate the one which contains θ. When the number of regions is too high, it would be preferable to use more efficient methods to conduct the search such as those described in [45] and [46].

The parameter space for which the explicit solution has been computed is bounded by

$$\begin{aligned}
-0.5 &\leq y_{k-i} \leq 10.5, \qquad i = 0, \ldots, 4 \\
-100 &\leq \Delta u_{k-i} \leq 100, \qquad i = 1, \ldots, 3 \\
-40 &\leq \Delta v_{k-i} \leq 40, \qquad i = 1, \ldots, 4 \\
-0.5 &\leq w_{k-1} \leq 10.5 \\
-0.5 &\leq u_{k-1} \leq 100.5 \\
-0.5 &\leq v_{k-1} \leq 40.5.
\end{aligned} \quad (40)$$

These limits arise from the physical characteristics and parameters of the real fuel cell. The constraints are for the air-flow rate from 35 to 100 slpm and for the oxygen excess from zero to eight, whereas suitable current demand ranges from 0 to 40 A. The prediction and control horizons were set at four and the weighting factor λ at 20.

The controller obtained has 221 different regions. Note that the number of regions is small enough so that the online evaluation can be done by performing a simple sequential search over the parameter space partition. A significantly greater number of regions would require more efficient search implementation methods [45], [46]. As for the fuel-cell system that we are dealing with, the sampling time was set at 10 ms (as indicated in Section IV). Once implemented in the PC104 650-MHz CPU, the maximum execution time of the explicit MPC law turned out to be 0.7035 ms, with an average execution time of 0.245 ms, as shown in Fig. 14, thereby ensuring real-time execution.

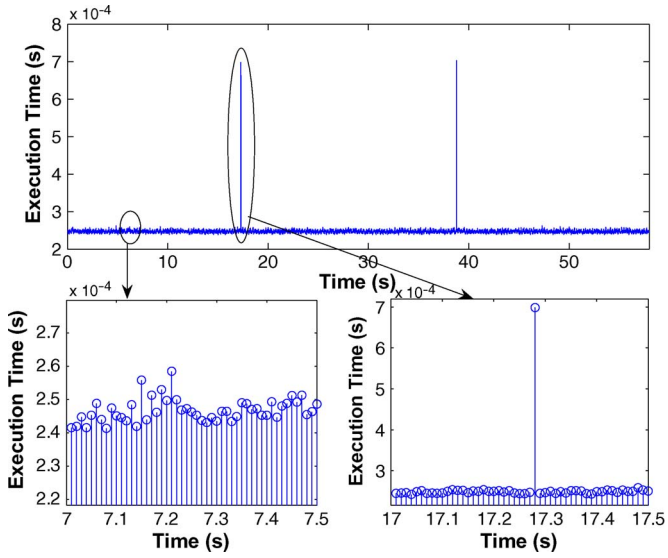

Fig. 14. Constrained explicit MPC execution times.

Regarding the closed-loop stability of the system, there is no particular risk of losing stability with the proposed controller parameters (i.e., horizons and weighting factors). Moreover, the controller has been tuned and tested under simulation so that the closed-loop response is both stable and adequate in terms of performance. Closed-loop stability can be enforced by using several known ingredients (see [44], [47], and [48]) which are sufficient, but not necessary, conditions. In fact, as the fuel cell is open-loop stable and the input signal is bounded, the closed-loop system is stable, at least in the bounded-input–bounded-output sense.

VI. Results and Discussions

This section is dedicated to the results obtained during experiments realized with the 1.2-kW PEM fuel-cell test bench. The two control strategies proposed in this paper are discussed and compared with each other and as with the manufacturer's control law as well.

A. Control Strategies

Fig. 15 shows the experimental results corresponding to the starvation avoidance control objective. The electronic load was programmed to demand current step series for the fuel cell, as shown in the upper graph, ranging from 15 to 25 A. The control objective was set to maintain a constant oxygen excess ratio of three. The lower graph shows that the controller maintains a stable λ_{O_2} with no steady-state errors. During the transients, particularly after abrupt load changes, λ_{O_2} suffers large drops

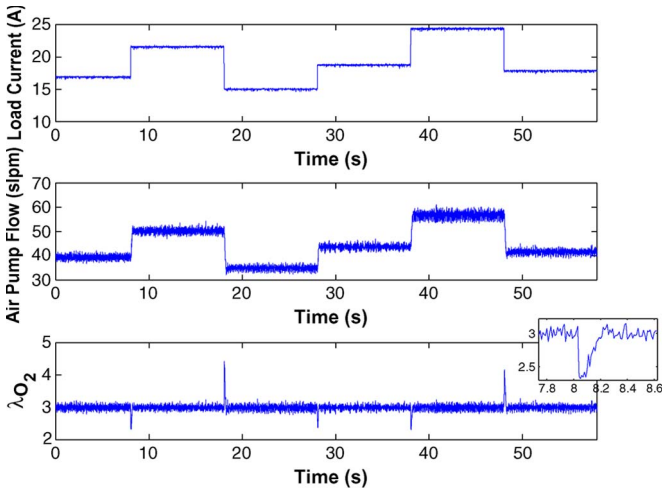

Fig. 15. Starvation-prevention criteria.

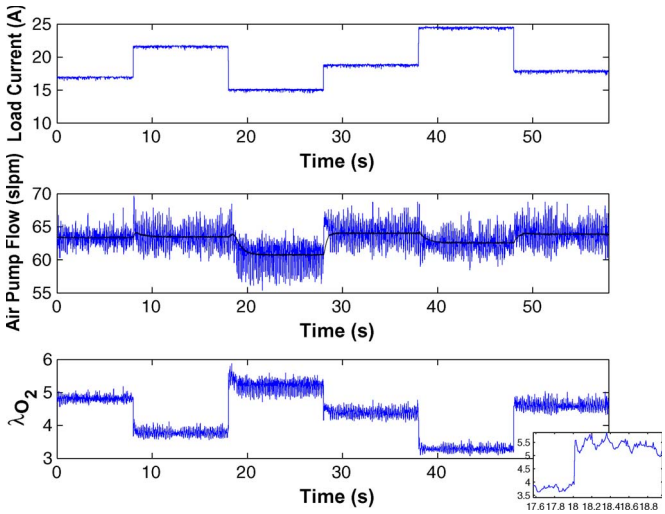

Fig. 16. Maximum-efficiency criteria.

mainly due to the fact that the electrochemical dynamics of a fuel cell prove to be various orders of magnitude higher than the fluid-dynamics response time (as indicated earlier in Section III). However, the controller shows a fast response in order to track the reference λ_{O_2}, which is reached in approximately 200 ms.

In order to test the maximum-efficiency control objective, an experiment with the same load step series was performed (see Fig. 16). Contrary to the starvation avoidance criterion, in which a fixed λ_{O_2} must be maintained, the oxygen excess ratio is now selected in order to obtain the maximum fuel-cell stack net power. As shown in the lower graph, oxygen excess ratio ranges from $\lambda_{O_2} = 3.2$ to $\lambda_{O_2} = 5.25$, seeking the "best path" for optimized fuel-cell operation, which is more extensively discussed in Section III (see also Fig. 20).

B. Transient Response

In order to compare the transient response capability of the explicit MPC proposed herein, the maximum efficiency objective was compared with the manufacturer's control law. To

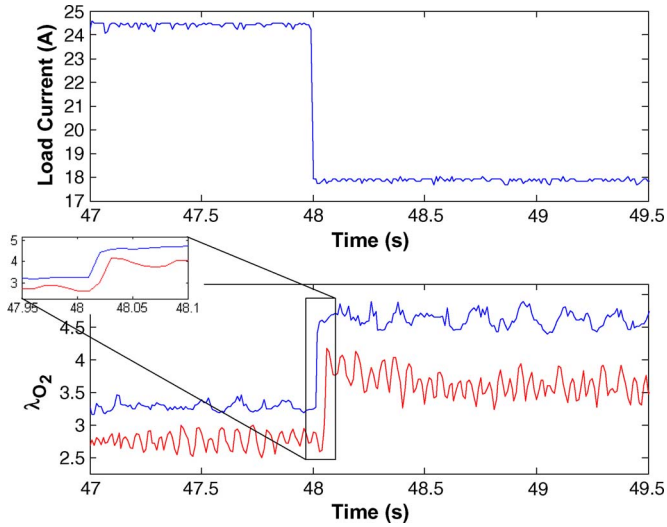

Fig. 17. Transient-response comparison.

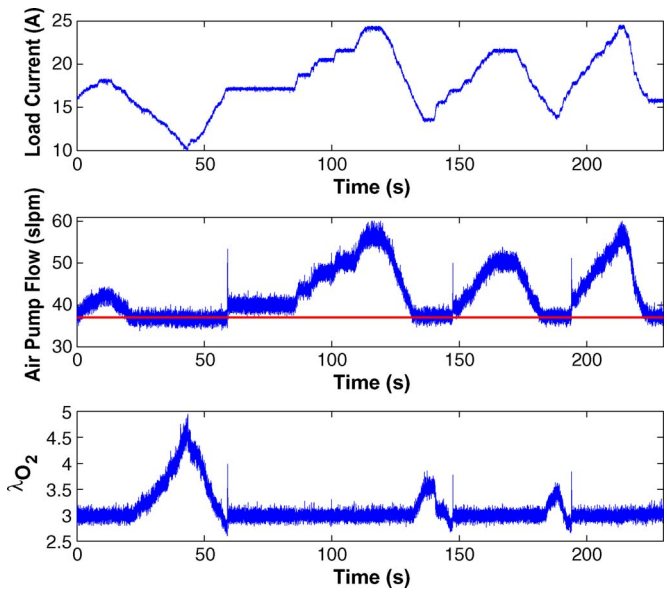

Fig. 18. Air-flow constraint.

that end, the experiment shown in Fig. 17 was conducted. As shown, the rise time corresponding to the controller proposed herein is approximately 15 ms for a stack current step of 6 A while the rise time in the manufacturer's law is 28 ms.

C. Constraints

As compressor working range limits of 37–100 slpm were imposed for the explicit MPC formulation, there are some situations in which the λ_{O_2} reference cannot be tracked. Such situations arise when the controller needs to track a reference λ_{O_2} which is outside the aforementioned constrained region. Fig. 18 shows that a value of $\lambda_{O_2} = 3$ could not be attained for the lowest stack current values. In those periods, the reference $\lambda_{O_2} = 3$ was not achieved, resulting in higher oxygen excess ratios.

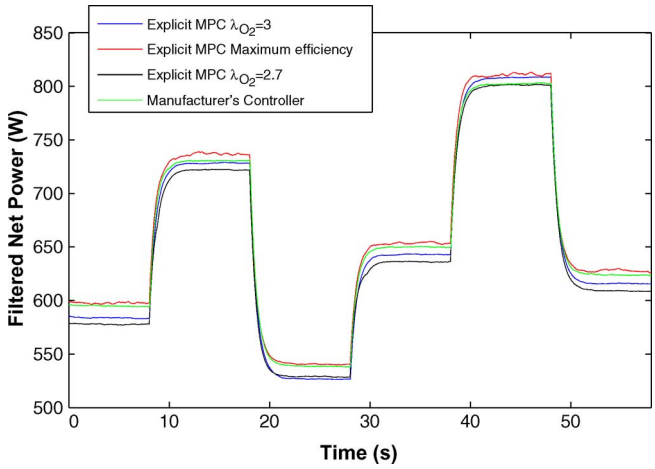

Fig. 19. Net-power comparison.

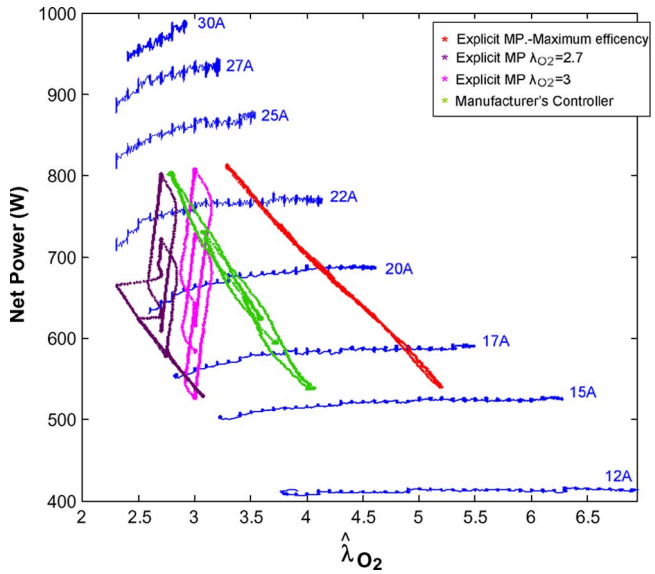

Fig. 20. Dynamic trajectories of the control objectives.

D. Efficiency

Finally, the efficiency of the control objectives discussed herein are compared. Therefore, four control objectives were tested for the stack current profile, as shown in Fig. 19: a starvation avoidance criterion maintaining fixed λ_{O_2} values of 2.7 and 3, a manufacturer's controller criterion, and a maximum efficiency criterion. Fig. 20 shows the filtered fuel-cell net power for the four aforementioned control objectives. The less-efficient objective turns out to be the one corresponding to a fixed $\lambda_{O_2} = 2.7$. As shown in Fig. 20, such a control objective is in a low-air-flow-rate region, which corresponds to a low fuel-cell system efficiency. Maintaining a fixed value of $\lambda_{O_2} = 3$ results in a more efficient criterion as the region in which the controller moves is closer to the optimal region. The manufacturer's law follows a path similar to the optimal path calculated herein but displaced to the left. The maximum efficiency control objective developed in this paper is thus the one which achieves better fuel-cell efficiency, as it follows the optimal path perfectly (see Fig. 20).

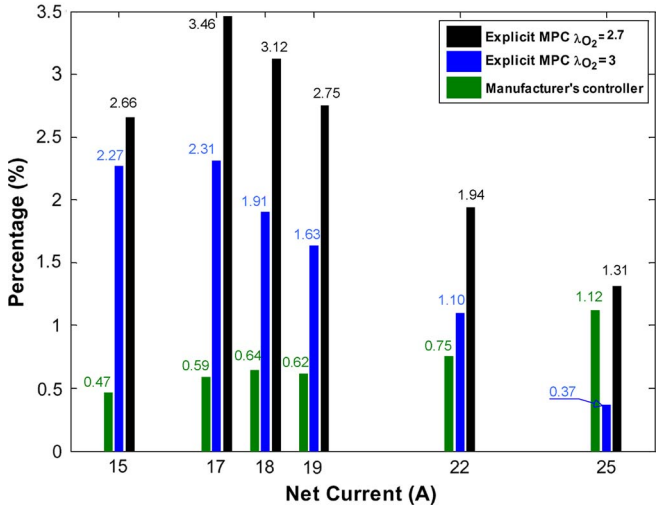

Fig. 21. Efficiency-improvement comparison.

In more specific terms, as shown in Fig. 21, the larger improvement percentages are obtained by comparing the maximum efficiency criterion with the criterion aimed at maintaining a fixed $\lambda_{O_2} = 2.7$, achieving an improvement of 3.46%. Furthermore, a maximum improvement of 1.10% was achieved on the manufacturer's law, constituting one of the main achievements of this paper.

VII. Concluding Remarks

In this paper, a real-time explicit MPC formulation has been implemented and validated on a 1.2-kW PEM fuel-cell test bench. Two control objectives have been proposed in order to manage the air supply of the fuel-cell system, respectively, aimed at avoiding oxygen starvation (maintaining a fixed λ_{O_2}) and maximizing fuel-cell efficiency. Such control objectives were compared with each other and with the manufacturer's built-in controller objective, showing improved transient responses and better fuel-cell efficiency in the case of the efficiency maximization objective. As the explicit controller proposed herein has only one tuning parameter, such a controller could simply be adapted to other similar fuel-cell systems. Future works will be focused on taking fuel-cell degradation into account, so that the controller can be adapted to consider parameter changes.

Acknowledgment

The authors would like to thank A. Oliva for his help in carrying out the experiments.

References

[1] P. Rodatz, G. Paganelli, A. Sciarretta, and L. Guzzella, "Optimal power management of an experimental fuel cell/supercapacitor powered hybrid vehicle," *Control Eng. Pract.*, vol. 13, no. 1, pp. 41–53, Jan. 2005.
[2] A. Stefanopoulou and K.-W. Suh, "Mechatronics in fuel cell systems," *Control Eng. Pract.*, vol. 15, no. 3, pp. 277–289, Mar. 2007.
[3] S. Lukic, J. Cao, R. Bansal, F. Rodriguez, and A. Emadi, "Energy storage systems for automotive applications," *IEEE Trans. Ind. Electron.*, vol. 55, no. 6, pp. 2258–2267, Jun. 2008.
[4] J.-W. Ahn and S.-Y. Choe, "Coolant controls of a PEM fuel cell system," *J. Power Sources*, vol. 179, no. 1, pp. 252–264, Apr. 2008.

[5] D. Chu and R. Jiang, "Performance of polymer electrolyte membrane fuel cell (PEMFC) stacks: Part I. Evaluation and simulation of an air-breathing PEMFC stack," *J. Power Sources*, vol. 83, no. 1/2, pp. 128–133, Oct. 1999.
[6] T. Okada, "Theory for water management in membranes for polymer electrolyte fuel cells: Part 1. The effect of impurity ions at the anode side on the membrane," *J. Electroanal. Chem.*, vol. 465, no. 1, pp. 1–17, Apr. 1999.
[7] S. Shimpalee, D. Spuckler, and J. V. Zee, "Prediction of transient response for a 25 m^2 PEM fuel cell," *J. Power Sources*, vol. 167, no. 1, pp. 130–138, May 2007.
[8] D. Mckay, J. Siegel, W. Ott, and A. Stefanopoulou, "Parameterization and prediction of temporal fuel cell voltage behavior during flooding and drying conditions," *J. Power Sources*, vol. 178, no. 1, pp. 207–222, Mar. 2008.
[9] J. Correa, F. Farret, L. Canha, and M. Simoes, "An electrochemical-based fuel-cell model suitable for electrical engineering automation approach," *IEEE Trans. Ind. Electron.*, vol. 51, no. 5, pp. 1103–1112, Oct. 2004.
[10] S. Jemei, D. Hissel, M.-C. Pera, and J. Kauffmann, "A new modeling approach of embedded fuel-cell power generators based on artificial neural network," *IEEE Trans. Ind. Electron.*, vol. 55, no. 1, pp. 437–447, Jan. 2008.
[11] L. Zhang, M. Pan, and S. Quan, "Model predictive control of water management in PEMFC," *J. Power Sources*, vol. 180, no. 1, pp. 322–329, May 2008.
[12] T. Nguyen and M. W. Knobbe, "A liquid water management strategy for PEM fuel cell stacks," *J. Power Sources*, vol. 114, no. 1, pp. 70–79, Feb. 2003.
[13] J. Pukrushpan, A. Stefanopoulou, and H. Peng, "Control of fuel cell breathing," *IEEE Control Syst. Mag.*, vol. 24, no. 2, pp. 30–46, Apr. 2004.
[14] P. Thounthong and P. Sethakul, "Analysis of a fuel starvation phenomenon of a PEM fuel cell," in *Proc. PCC*, Nagoya, Japan, 2007, pp. 731–738.
[15] J. Prukushpan, A. Stefanopoulou, and H. Peng, *Control of Fuel Cell Power Systems: Principles, Modelling and Analysis and Feedback Design*. New York: Springer-Verlag, 2004, ser. Advances in Industrial Control.
[16] P. Rodatz, G. Paganelly, and L. Guzzella, "Optimizing air supply control of a PEM fuel cell system," in *Proc. Amer. Control Conf.*, Denver, CO, Jun. 2003, pp. 2043–2048.
[17] C. Bao, M. Ouyang, and B. Yi, "Modeling and control of air stream and hydrogen flow with recirculation in a PEM fuel cell system—II: Linear and adaptive nonlinear control," *Int. J. Hydrogen Energy*, vol. 31, no. 13, pp. 1897–1913, Oct. 2006.
[18] Y. Yang, F.-C. Wang, H.-P. Chang, Y.-W. Ma, and B.-J. Weng, "Low power proton exchange membrane fuel cell system identification and adaptive control," *J. Power Sources*, vol. 164, no. 2, pp. 761–771, Feb. 2007.
[19] M. Tekin, D. Hissel, M.-C. Pera, and J.-M. Kauffmann, "Energy consumption reduction of a PEM fuel cell motor-compressor group thanks to efficient control laws," *J. Power Sources*, vol. 156, no. 1, pp. 57–63, May 2006.
[20] M. Tekin, D. Hissel, M.-C. Pera, and J. Kauffmann, "Energy-management strategy for embedded fuel-cell systems using fuzzy logic," *IEEE Trans. Ind. Electron.*, vol. 54, no. 1, pp. 595–603, Feb. 2007.
[21] A. Saengrung, A. Abtahi, and A. Zilouchian, "Neural network model for a commercial PEM fuel cell system," *J. Power Sources*, vol. 172, no. 2, pp. 749–759, Oct. 2007.
[22] M. El-Sharkh, A. Rahman, and M. Alam, "Neural networks-based control of active and reactive power of a stand-alone PEM fuel cell plant," *J. Power Sources*, vol. 135, no. 1/2, pp. 88–94, Sep. 2004.
[23] M. Danzer, J. Wilhelm, H. Ascheman, and E. Hofer, "Model-based control of cathode pressure and oxygen excess ratio of a PEM fuel cell system," *J. Power Sources*, vol. 176, no. 2, pp. 515–522, Feb. 2008.
[24] A. Vahidi, A. Stefanopoulou, and H. Peng, "Model predictive control for starvation prevention in a hybrid fuel cell system," in *Proc. IEEE Amer. Control Conf.*, 2004, pp. 834–839.
[25] J. Sun and I. Kolmanovsky, "A robust load governor for fuel cell oxygen starvation prevention," in *Proc. IEEE Amer. Control Conf.*, 2004, pp. 828–833.
[26] G. Liu, J. Zhang, and Y. Sun, "High frequency decoupling strategy for the PEM fuel cell hybrid system," *Int. J. Hydrogen Energy*, vol. 33, no. 21, pp. 6253–6261, Nov. 2008.
[27] A. Vahidi, A. Stefanopoulou, and H. Peng, "Current management in a hybrid fuel cell power system: A model-predictive control approach," *IEEE Trans. Control Syst. Technol.*, vol. 14, no. 6, pp. 1047–1057, Nov. 2006.
[28] M. Ortúzar, J. Moreno, and J. Dixon, "Ultracapacitor-based auxiliary energy system for an electric vehicle: Implementation and evaluation," *IEEE Trans. Ind. Electron.*, vol. 54, no. 4, pp. 2147–2156, Aug. 2007.
[29] P. Thounthong, S. Rael, and B. Davat, "Control strategy of fuel cell and supercapacitors association for a distributed generation system," *IEEE Trans. Ind. Electron.*, vol. 54, no. 6, pp. 3225–3233, Dec. 2007.
[30] C. Ramos-Paja, C. Bordons, A. Romero, R. Giral, and L. Martínez-Salamero, "Minimum fuel consumption strategy for PEM fuel cells," *IEEE Trans. Ind. Electron.*, vol. 56, no. 3, pp. 685–696, Mar. 2009.
[31] C. Woo and J. Benziger, "PEM fuel cell current regulation by fuel feed control," *Chem. Eng. Sci.*, vol. 62, no. 4, pp. 957–968, Feb. 2007.
[32] A. J. del Real, A. Arce, and C. Bordons, "Development and experimental validation of a PEM fuel cell dynamic model," *J. Power Sources*, vol. 173, no. 1, pp. 310–324, Nov. 2007.
[33] A. Bemporad, M. Morari, V. Dua, and E. Pistikopoulos, "The explicit linear quadratic regulator for constrained systems," *Automatica*, vol. 38, no. 1, pp. 3–20, Jan. 2002.
[34] A. Bemporad, M. Morari, V. Dua, and E. Pistikopoulos, "Corrigendum to: 'The explicit linear quadratic regulator for constrained systems' [Automatica 38(1)(2002)3–20]," *Automatica*, vol. 39, no. 10, pp. 1845–1846, Oct. 2003.
[35] J. Larminie and A. Dicks, *Fuel Cell Systems Explained*., 2nd ed. Hoboken, NJ: Wiley, 2003.
[36] J. Gruber, M. Doll, and C. Bordons, "Design and experimental validation of a constrained MPC for the air feed of a fuel cell," *Control Eng. Pract.*, vol. 17, no. 8, pp. 874–885, Aug. 2009.
[37] A. Arce, A. J. del Real, and C. Bordons, "Application of constrained predictive control strategies to a PEM fuel cell benchmark," in *Proc. Eur. Control Conf.*, 2007, pp. 2985–2990.
[38] C. Bordons, A. Arce, and A. del Real, "Constrained predictive control strategies for PEM fuel cells," in *Proc. IEEE Amer. Control Conf.*, Minneapolis, MN, 2006, pp. 2486–2491.
[39] J. Amphlett, R. Baumert, R. Mann, B. Peppley, P. Roberge, and T. Harris, "Performance modeling of the Ballard Mark IV solid polymer electrolyte fuel cell," *J. Electrochem. Soc.*, vol. 142, no. 1, pp. 9–15, Jan. 1995.
[40] M. S. Al-Baghdadi, "Modelling of proton exchange membrane fuel cell performance based on semi-empirical equations," *Renew. Energy*, vol. 30, no. 10, pp. 1587–1599, Aug. 2005.
[41] T. Springer, T. Zawodzinski, and S. Gottesfeld, "Polymer electrolyte fuel cell model," *J. Electrochem. Soc.*, vol. 138, no. 8, pp. 2334–2342, 1991.
[42] T. Fuller and J. Newmann, "Water and thermal management in solid-polymer-electrolyte fuel cells," *J. Electrochem. Soc.*, vol. 140, no. 5, pp. 1218–1225, 1993.
[43] C. Bao, M. Ouyang, and B. Yi, "Modeling and control of air stream and hydrogen flow with recirculation in a PEM fuel cell system—I. Control-oriented modeling," *Int. J. Hydrogen Energy*, vol. 31, no. 13, pp. 1879–1896, Oct. 2006.
[44] E. F. Camacho and C. Bordons, *Model Predictive Control*. London, U.K.: Springer-Verlag, 2004.
[45] T. Johansen and A. Grancharova, "Approximate explicit constrained linear model predictive control via orthogonal search tree," *IEEE Trans. Autom. Control*, vol. 48, no. 5, pp. 810–815, May 2003.
[46] P. Tøndel, T. Johansen, and A. Bemporad, "Evaluation of piecewise affine control via binary search tree," *Automatica*, vol. 39, no. 5, pp. 945–950, May 2003.
[47] D. Mayne, J. Rawlings, C. Rao, and P. Scokaert, "Constrained model predictive control: Stability and optimality," *Automatica*, vol. 36, no. 6, pp. 789–814, Jun. 2000.
[48] D. Mayne, "Control of constrained dynamic systems," *Eur. J. Control*, vol. 7, no. 2/3, pp. 87–99, 2001.

Alicia Arce was born in Sevilla, Spain, in 1980. She received the M.Eng. degree in automatic systems and robotics from the Universidad de Sevilla, Sevilla, in 2007, where she has been working toward the Ph.D. degree in the Departamento de Ingeniería de Sistemas y Automática since 2005, where she is involved in several projects related with fuel cells.

Currently, her work is focused on hybrid vehicles propelled by proton exchange membrane fuel cells.

Alejandro J. del Real was born in Sevilla, Spain, in 1981. He received the M.Eng. in automatic systems and robotics from the Universidad de Sevilla, Sevilla, in 2007, where he has been working toward the Ph.D. degree in the Departamento de Ingeniería de Sistemas y Automática since 2005.

His research interests include modeling and control of hybrid systems which integrate fuel cells and renewable power sources. He has also been involved in some other fuel-cell-related projects.

Carlos Bordons (M'98) received the Ph.D. degree in electrical engineering from the Universidad de Sevilla, Sevilla, Spain, in 1994.

He joined the Escuela Superior de Ingenieros, Universidad de Sevilla, as an Assistant Professor in 1989, where he is currently a Full Professor. He has worked in different projects in collaboration with industry in fields such as control of steam generators in sugar factories, simulation and optimization of oil pipeline networks, automation of copper furnaces, or modeling and control of fuel-cell systems. He is a coauthor of the books *Model Predictive Control in the Process Industry* and *Model Predictive Control* (first and second editions) published by Springer-Verlag, London. He is the holder of two patents related to his fields of interest. His current research interests include advanced process control, particularly model predictive control and its application to fuel-cell-based systems.

Dr. Bordons was elected as a European Union Control Association Council Member in 2007.

Daniel R. Ramírez was born in Spain in 1972. He received the M.Eng. and Ph.D. degrees in computer engineering from the Universidad de Sevilla, Sevilla, Spain, in 1996 and 2002, respectively.

From 1997 to 1999, he was a Research Assistant with the Departamento de Ingeniería de Sistemas y Automática, Universidad de Sevilla, where he has been an Associate Professor since 2009. He has authored and coauthored more than 25 technical papers in international journals and conference proceedings. He has participated in several European projects. His current research interests include model predictive control, process control, soft computing techniques, and mobile robotics.